Dynamics and structure of decaying shallow dipolar vortices

M. Duran-Matute,[1] J. Albagnac,[2] L. P. J. Kamp,[1] and G. J. F. van Heijst[1]
[1]*Department of Applied Physics and J.M. Burgers Centre, Eindhoven University of Technology, P.O. Box 513, 5600 MB Eindhoven, The Netherlands*
[2]*IMFT, Université de Toulouse, Allée Camille Soula, 31400 Toulouse, France*

The current work reports on a numerical and experimental study of the evolution of decaying dipolar vortices in a shallow fluid layer. The dynamics and the structure of such vortices are investigated as a function of both their Reynolds number Re and the aspect ratio of vertical and horizontal length scales δ. By quantifying the strength of the secondary motions (vertical motions and nonzero horizontal divergence) with respect to the swirling motions of the primary vortex cores, it was found that the three-dimensionality of a shallow ($\delta \ll 1$) dipolar vortex only depends on a single parameter: δ^2 Re. Depending on the value of this parameter, three flow regimes are observed for shallow dipolar vortices: (1) a quasi-two-dimensional regime where the structure of the dipolar vortex remains almost unchanged throughout its lifetime, (2) a transitional regime where the structure presents some three-dimensional characteristics but remains coherent, and (3) a three-dimensional regime where the structure of the dipolar vortex acquires a complicated three-dimensional shape with a persistent spanwise vortex at its front.

I. INTRODUCTION

It is commonly assumed that the small depth of shallow flows constrains the magnitude of the vertical velocity,[1,2] leading to mainly horizontal quasi-two-dimensional (Q2D) flows. One of the characteristics of Q2D flows is their self-organization into large coherent structures. This phenomenon has been observed in a shallow layer of fluid by, for example, Sous *et al.*[3,4] In their studies, an impulsive turbulent jet was introduced into a fluid initially at rest. For small fluid depths, it was observed that the vertical motions are damped and that the turbulent jet evolves into a large coherent dipolar vortex.

However, several recent studies have demonstrated that shallow dipolar vortices present a complicated three-dimensional (3D) structure with vertical velocities that do not scale linearly with the aspect ratio. For instance, Lin *et al.*[5] studied the 3D structure of vortex dipoles generated by a piston-nozzle arrangement and observed a secondary vortex, which is orthogonal and just ahead of the primary dipole. Sous *et al.*[3,4] also observed the presence of a spanwise vortex at the front of the dipolar vortex for certain regions of their parameter space. Akkermans *et al.*[6,7] investigated numerically and experimentally the evolution of electromagnetically forced vortex dipoles. Besides observing a spanwise vortex in front of the vortex dipole, they also measured large non-negligible vertical velocities—which impair the two-dimensionality of the flow—in the vortex cores of the dipole. A spanwise vortex was also observed by Lacaze *et al.*,[8] who performed laboratory experiments on shallow laminar dipolar vortices generated by two closing flaps. As a continuation of those experiments, Lacaze and co-workers have set out to investigate thoroughly the dynamics of the spanwise vortex (personal communication). That work has served as an inspiration for the current paper.

The importance of vertical flows—and by continuity, radial flows—for the evolution of shallow monopolar vortices has been previously studied using numerical simulations.[9,10] These previous studies have shown that indeed the small aspect ratio promotes a decrease in the magnitude of vertical motions inside the monopolar vortices. In addition, it was shown that this magnitude depends also on the Reynolds number. Moreover, for shallow axisymmetric swirl flows, only the parameter δ^2 Re—where Re is the Reynolds number and δ is the flow aspect ratio—characterizes the flow.[10]

In the present paper, we study numerically and experimentally the two-dimensionality of a decaying dipolar vortex as a function of both the Reynolds number Re and the aspect ratio δ of the initial dipole. The aim of the current paper is twofold: (1) to explain previous seemingly contradictory experimental results on the two-dimensionality of shallow flows[3]—in particular, the results for dipolar vortices, that can still present complicated 3D structures in very shallow layers[6] even if shallowness has been shown to promote its two-dimensionality;[3,4] and (2) to test in a somewhat more complicated flow, namely, the dipolar vortex structure, the scaling properties previously obtained for an axisymmetric monopolar vortex.[10]

High-resolution 3D numerical simulations, together with the use of the so-called λ_2 vortex detection criterion,[11,12] have revealed the full 3D structure of the dipole, providing new insight into the dynamics of shallow flows. Of special interest is the effect that secondary motions have on the 3D structure of the dipolar vortex as the parameter δ^2 Re is increased. Furthermore, results from laboratory experiments show good agreement with the numerical simulations and give confidence on the robust character of the numerical results.

The paper is organized as follows. In Sec. II, the prob-

lem is formulated and the nondimensional parameters characterizing the flow are defined. Section III is devoted to the numerical study of an initially Q2D dipolar vortex, where, first, the numerical simulations are described. In Sec. III A the strength of the 3D motions are quantified. Then, Sec. III B presents the three different flow regimes observed in the range of parameters studied. Finally, in Sec. IV the laboratory experiments are presented and qualitatively compared with the numerical results. A discussion of the results and some conclusions are presented in Sec. V.

II. STATEMENT OF THE PROBLEM

We study a decaying symmetric dipolar vortex—a compact structure consisting of two counter-rotating vortex cores with equal strength and size—in a shallow fluid layer. Due to the strong interaction of the vortex cores, this structure propagates along a straight line.[13]

The flow is considered to be governed by the Navier–Stokes equation,

$$\frac{\partial \boldsymbol{v}}{\partial t} + (\boldsymbol{v}\cdot\boldsymbol{\nabla})\boldsymbol{v} = -\frac{1}{\rho}\boldsymbol{\nabla} P + \nu\nabla^2\boldsymbol{v}, \tag{1}$$

and the continuity equation for an incompressible fluid,

$$\boldsymbol{\nabla}\cdot\boldsymbol{v} = 0, \tag{2}$$

with $\boldsymbol{v}$ the velocity of the fluid, t the time, ρ the density of the fluid, P the pressure, and ν the kinematic viscosity of the fluid. The motion of the fluid is described in Cartesian coordinates $\boldsymbol{x}=(x,y,z)$ with x the direction of propagation of the dipole, y the spanwise direction, and z the vertical direction. The velocity and vorticity vectors are then written as $\boldsymbol{v}=(u,v,w)$ and $\boldsymbol{\omega}=\boldsymbol{\nabla}\times\boldsymbol{v}=(\omega_x,\omega_y,\omega_z)$, respectively.

To nondimensionalize Eqs. (1) and (2), the following nondimensional variables, which are denoted by primes, are defined:

$$\boldsymbol{v}' = \frac{\boldsymbol{v}}{U_0}, \quad \boldsymbol{\omega}' = \frac{R_0}{U_0}\boldsymbol{\omega}, \quad t' = \frac{U_0}{R_0}t, \quad P' = \frac{P}{\rho U_0^2},$$
$$x' = \frac{x}{R_0}, \quad y' = \frac{y}{R_0}, \quad z' = \frac{z}{H}, \tag{3}$$

where U_0 is the initial propagation speed of the dipole, R_0 is the initial radius of the dipole, and H is the depth of the fluid layer. Then, substituting Eq. (3) into Eqs. (1) and (2) yields

$$\frac{\partial \boldsymbol{v}'}{\partial t'} + (\boldsymbol{v}'\cdot\tilde{\boldsymbol{\nabla}})\boldsymbol{v}' = -\tilde{\boldsymbol{\nabla}}P' + \frac{1}{\mathrm{Re}}\tilde{\boldsymbol{\nabla}}^2\boldsymbol{v}', \tag{4}$$

$$\tilde{\boldsymbol{\nabla}}\cdot\boldsymbol{v} = 0, \tag{5}$$

where

$$\tilde{\boldsymbol{\nabla}} \equiv \left(\frac{\partial}{\partial x'}, \frac{\partial}{\partial y'}, \frac{1}{\delta}\frac{\partial}{\partial z'}\right), \tag{6}$$

and where the Reynolds number

$$\mathrm{Re} \equiv \frac{U_0 R_0}{\nu} \tag{7}$$

and the aspect ratio

$$\delta \equiv \frac{H}{R_0} \tag{8}$$

are the two nondimensional parameters characterizing the flow. To simplify notation, the primes will be omitted from here on, and only the nondimensional variables will be used.

III. NUMERICAL SIMULATIONS

In the present study, the governing Eqs. (1) and (2) are solved numerically using a finite-element code (see Ref. 14). The numerical domain is $-9\le x\le 21$, $0\le y\le 15$, $0\le z\le 1$. It has been previously observed that this domain size is large enough as not to affect the results of the simulations due to the effect of lateral boundaries.[7]

As boundary conditions, a no-slip boundary condition is imposed at the bottom, whereas the surface is stress-free, flat, and rigid so that free-surface deformations are excluded. A stress-free condition is implemented for all lateral boundaries in order to further reduce the possible influence of these boundaries.

The flow is initialized in the horizontal plane with a Lamb–Chaplygin dipolar vortex[15] with unit radius and a Poiseuille-like vertical structure according to

$$\boldsymbol{U}_{LC}(x,y) = \left(1 + \frac{\partial\psi}{\partial y}, -\frac{\partial\psi}{\partial x}, 0\right)\sin\left(\frac{\pi z}{2}\right),$$

where the streamfunction ψ is defined as

$$\psi(r,\theta) = \begin{cases} -\dfrac{2}{\mu_1 J_0(\mu_1)} J_1(\mu_1 r)\sin\theta, & r\le 1 \\ -\left(r - \dfrac{1}{r}\right)\sin\theta, & r > 1, \end{cases} \tag{9}$$

with J_0 and J_1 the zeroth and first order Bessel functions of the first kind and μ_1 the first zero of J_1. Note that $x=r\cos\theta$ and $y=r\sin\theta$ so that $r=\sqrt{x^2+y^2}$ and $\theta=\tan^{-1}(y/x)$.

The Lamb–Chaplygin vortex dipole was chosen because of its resemblance to horizontal slices of experimentally created dipolar vortices.[3,4,16–18] The vertical Poiseuille-like structure was chosen since it seems to be a realistic profile for time-dependent shallow flows.[9]

Due to the symmetry with respect to the vertical plane $y=0$, only the evolution of one half of the dipole ($y>0$) is simulated. However, for visualization purposes, the full dipolar vortex is reconstructed in the figures shown in this section.

The spatial resolution was checked by performing several simulations for two points in the (Re,δ) parameter space with increasing resolution until no significant differences were observed. This check resulted in a computational domain discretized with approximately 43 000 unstructured mesh elements. A finer mesh was used in regions where high velocity gradients were expected. In addition, mesh elements in the vertical direction are between three and nine times

TABLE I. Values of the Reynolds number Re and the aspect ratio δ used in the numerical simulations.

δ	Re
0.1	200, 300, 400, 800
0.2	50, 70, 100, 150, 200, 260, 500, 1000
0.3	25, 40, 50, 89, 100, 200, 222, 260
0.7	4, 8, 16, 40, 70, 90, 145

smaller than the ones in the horizontal direction to resolve vertical gradients with sufficient resolution. In this way, the equations were solved for approximately 955 000 degrees of freedom.

Time steps were determined by the numerical code using variable-order variable-step-size backward differentiation formulas[14] with the time resolution computed from the relative and absolute error tolerances. The values for such error tolerances were deduced by performing several simulations with decreasing tolerance until no significant difference between the simulations was observed.

The parameter space was explored by performing several numerical simulations for different values of the Reynolds number Re and the aspect ratio δ as shown in Table I.

A. Quantitative characterization of the flow

As the dipolar vortex is left to evolve freely, secondary motions arise in the form of upwelling or downwelling in the vortex cores[6,7] and in the form of a spanwise vortex at the front of the dipole.[3,6–8] To quantify the strength of these secondary motions, we consider the following quantities: (1) the normalized horizontal divergence at the surface ($z=1$),

$$\Delta(t)=\frac{\int_{A_H}|\boldsymbol{\nabla}\cdot\boldsymbol{v}(x,y,1,t)|dxdy}{\int_{A_H}|\boldsymbol{k}\cdot\boldsymbol{\nabla}\times\boldsymbol{v}(x,y,1,t)|dxdy} \tag{10}$$

(as previously used by Akkermans *et al.*[7]) and (2) the normalized kinetic energy of the vertical velocity component in the vertical symmetry plane $y=0$,

$$Q_z(t)=\frac{\int_{A_V}w^2(x,0,z,t)dxdz}{\int_{A_V}u^2(x,0,z,t)dxdz} \tag{11}$$

(as previously used by Sous *et al.*[3]), where A_H is the horizontal area of the numerical domain, A_V is the area of the vertical symmetry plane, and $\boldsymbol{k}$ is the unit vector in the z-direction. In particular, we focus on the maximum in time of these two quantities: $\max(\Delta)$ and $\max(Q_z)$.

The surface $z=1$ was chosen to evaluate the horizontal divergence Δ since $w=0$ on this plane, and hence, the divergence is the only signature of the secondary motions. Similarly, in the vertical symmetry plane ($y=0$), the vertical velocity is the only signature of the secondary motions.

To quantify the strength of the secondary motions in an axisymmetric monopolar vortex, the flow can be easily decomposed, using cylindrical coordinates, into the primary motion in the azimuthal direction and secondary motions in the radial directions (see, e.g., Refs. 9 and 10). For the case of the monopolar vortex, the horizontal divergence is related

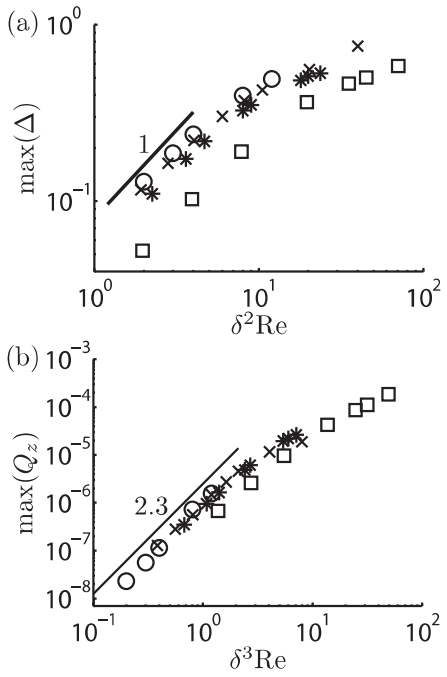

FIG. 1. Strength of the secondary motions as compared to the primary motions: (a) maximum of the normalized horizontal divergence at the surface as a function of δ^2 Re; (b) maximum of the normalized kinetic energy of the vertical velocity component in the vertical symmetry-plane as a function of δ^3 Re. The symbols denote simulations for different values of Re and δ=0.1 (○), δ=0.2 (×), δ=0.3 (*), and δ=0.7 (□). The solid lines represent the different scalings.

to the radial velocity, and hence, it only depends on δ^2 Re for $\delta \ll 1$. On the other hand, the magnitude of the vertical velocity only depends on δ^3 Re (see Ref. 10).

Figure 1(a) shows the maximum of the normalized horizontal divergence, $\max(\Delta)$, as a function of δ^2 Re. A collapse of the curves for δ=0.1, δ=0.2, and less clearly for δ=0.3 is observed. This collapse indicates—as for the monopolar vortex[10]—that shallow dipoles are characterized by only one nondimensional parameter: δ^2 Re, provided that $\delta \ll 1$. Indeed, the results given by simulations with δ=0.7 do not collapse with the curves described by the results for simulations with δ=0.1 and 0.2 since δ=0.7 is not small enough (i.e., the flow is not shallow enough) for the flow evolution to depend solely on the parameter δ^2 Re. In addition, the graph clearly shows the existence of a scaling regime for $\delta^2\,\mathrm{Re} \lesssim 6$, where $\max(\Delta) \propto \delta^2$ Re. From a comparison with a monopolar vortex, the scaling $\max(\Delta) \propto \delta^2$ Re implies that the flow is dominated by viscosity in this regime and that the secondary motions can be neglected. On the other hand, inertia dominates over viscous forces outside this regime.

In Fig. 1(b), the maximum of the normalized kinetic energy associated with the vertical velocity $\max(Q_z)$ is plotted as a function of δ^3 Re. Again, a collapse is observed for the curves described by the results of the numerical simulations with δ=0.1, 0.2, and 0.3, indicating that the magnitude of the vertical velocity depends only on δ^3 Re. In contrast, the results from the simulations with δ=0.7 do not collapse to the same curve. As for the monopolar vortex,[10] a scaling regime is found for $\delta^3\,\mathrm{Re} \lesssim 1$ although the exponent is somewhat

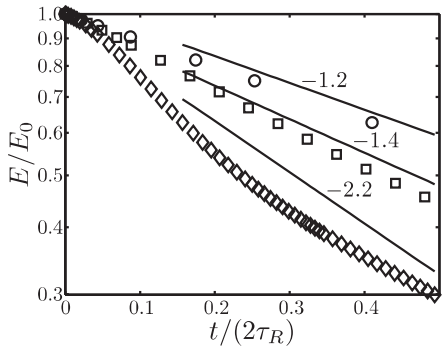

FIG. 2. Numerically obtained kinetic energy decay at the surface $z=1$ for three different simulations with $\delta=0.2$: Re=50 (○), Re=200 (□), and Re=500 (◇).

larger for the dipolar vortex. Outside this scaling regime, the secondary motion cannot be neglected, and hence the flow must be considered as 3D.

A few simulations with different initial vertical profiles, including a vertical profile which is independent of the vertical coordinate, were performed. It was observed that the scaling in the viscosity-dominated regime is independent of the initial vertical velocity profile. In contrast, the trend outside this regime depends on the initial vertical velocity profile. However, the viscous regime and the inertia-dominated regime never show the same scaling, implying that the two regimes are easily distinguishable.

To further characterize the flow, we calculate the typical decay time τ_D by fitting an exponential decay to the normalized kinetic energy associated with the horizontal velocity components at the surface $z=1$,

$$\frac{E(t)}{E_0}=\frac{\int_{A_H}[u^2(x,y,1,t)+v^2(x,y,1,t)]dxdy}{\int_{A_H}[u^2(x,y,1,0)+v^2(x,y,1,0)]dxdy}. \tag{12}$$

The decay time τ_D is then compared with the Rayleigh decay time,

$$\tau_R=\frac{4}{\pi^2}\delta^2\,\mathrm{Re} \tag{13}$$

[equivalent to $4H^2/(\pi^2\nu)$ in dimensional units] being the typical decay time for shallow flows dominated by bottom friction.[9,19]

Figure 2 shows the normalized kinetic energy as a function of time (normalized by the Rayleigh decay time τ_R) for simulations with $\delta=0.2$ and Re=50, 200, and 500 detailed in Sec. III B.

By fitting an exponential curve to the evolution of the kinetic energy, it can be seen that for small Reynolds numbers (e.g., Re=50), the characteristic decay time $\tau_D\sim\tau_R/1.2$ is close to the Rayleigh decay time. However, as the Reynolds number increases and the flow becomes 3D, the decay time becomes much shorter: $\tau_D\sim\tau_R/1.4$ for Re =200 and $\tau_D\sim\tau_R/2.2$ for Re=500. For Re=50 the difference between τ_D and τ_R is probably due to horizontal diffusion, which enhances the viscous decay. However, for larger values of Re the difference between τ_D and τ_R is due to the 3D dynamics of the flow: the advection of fluid by the secondary

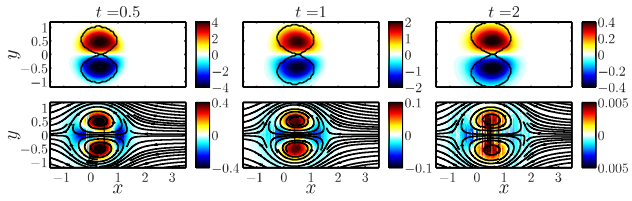

FIG. 3. (Color online) Evolution of a dipolar vortex at the surface ($z=1$) for a simulation with Re=50 and $\delta=0.2$ (δ^2 Re=2) at times $t=0.5$,1 and 2. Top row: the color/shade denotes the vertical vorticity component ω_z, and the black contour denotes the boundary of the vortex cores given by the $\lambda_2=0$ isoline. Lower row: the color/shade denotes the horizontal divergence and the black lines denote the flow lines tangential to the horizontal velocity components in the reference frame comoving with the vortex dipole.

motion toward a thin boundary layer at the bottom.[20] This advection increases the damping rate, like the Ekman boundary layers do for flows subjected to background rotation; see, for example, Ref. 2.

B. Flow regimes for shallow dipolar vortices

For the simulations of shallow dipoles ($\delta=0.1,0.2,0.3$), three qualitatively different flow regimes were observed in the range of Re-values investigated. Since the characteristics of shallow dipoles depend exclusively on the value of δ^2 Re, we base the description of the different regimes on the simulations with $\delta=0.2$, which are characteristic for simulations with other aspect ratios much smaller than unity (e.g., $\delta=0.1$ and 0.3). As δ approaches unity (e.g., $\delta=0.7$), the characteristics of the flow depend both on the values of δ and Re; it is not within the scope of the current work to analyze such cases.

The description of the three flow regimes for shallow dipolar vortices is mainly based on the 3D structure of dipolar vortex. To determine this structure, we used the λ_2 vortex detection criterion proposed by Jeong and Hussain[11] that allows to find the locations of local pressure minima in the flow that correspond to the presence of vortices. This detection criterion consists in calculating the real eigenvalues $\lambda_1\geq\lambda_2\geq\lambda_3$ of the symmetric tensor $\boldsymbol{S}^2+\boldsymbol{\Omega}^2$, where $\boldsymbol{S}$ and $\boldsymbol{\Omega}$ are the symmetric and antisymmetric components of $\boldsymbol{\nabla v}$, respectively. Then, the sectional pressure minimum induced by a vortex corresponds to regions where the second eigenvalue of $\boldsymbol{S}^2+\boldsymbol{\Omega}^2$ is negative: $\lambda_2<0$. Hence, the 3D boundary of a vortical structure is given by the isosurface $\lambda_2=0$. For more details, see also Ref. 12.

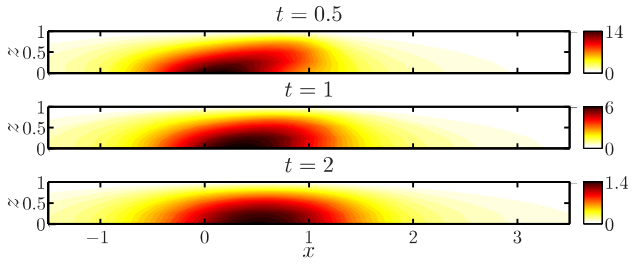

FIG. 4. (Color online) Evolution of the flow in the vertical symmetry plane ($y=0$) for a simulation with Re=50 and $\delta=0.2$ (δ^2 Re=2) at times $t=0.5$, 1, and 2. The color/shade denotes the spanwise vorticity component ω_y.

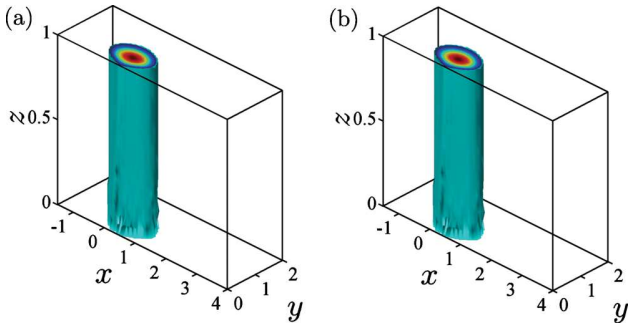

FIG. 5. (Color online) 3D structure of half of the dipolar vortex ($y>0$) for two simulations at time $t=1$. (a) Re=50 and $\delta=0.2$ (δ^2 Re=2). (b) Re=25 and $\delta=0.3$ (δ^2 Re=2.25). The structure is given by the isosurface $\lambda_2=0$ following the λ_2-criterion.

1. Q2D flow regime (δ^2 Re$\lesssim$6)

Figure 3 shows the evolution of the dipolar vortex for a simulation corresponding to Re=50 and $\delta=0.2$ (δ^2 Re=2). In the top row of Fig. 3, colors/shades denote the magnitude of the vertical vorticity ω_z and the black contour denotes the boundary of the vortex dipole as given by λ_2-criterion for $t=0.5$, 1, and 2 at the surface ($z=1$). As can be seen from the vertical vorticity ω_z distribution, the structure of the vortex dipole remains coherent. This is also reflected by the boundary of each vortex core, which describes approximately a circle throughout the flow evolution. In fact, only a weak increment, due to diffusion, in the size of the structure can be perceived.

In the lower row of Fig. 3, the colors/shades denote the horizontal divergence ($\partial u/\partial x+\partial v/\partial y$) and the black lines indicate the instantaneous flow lines tangential to the horizontal velocity components in the reference frame comoving with the dipolar vortex. By comparing the top and lower rows in Fig. 3, it can be observed that, at the surface ($z=1$), the positions of the primary vortex cores delineated by the $\lambda_2=0$ isoline correspond to areas of positive horizontal divergence. It is already known that a vortex with its rotation axis normal to a solid bottom induces an upwelling from the Bödewadt boundary layer into the vortex core.[20] Then, this upwelling induces a radial diverging flux at the surface. Downwelling areas are associated with converging fluxes, which are found close to the saddle type stagnation points at the front and at the rear of the dipolar vortex on its symmetry axis.

In the lower row of Fig. 3, the flow lines tangential to the horizontal velocity components define quasi-closed loops around two focal points corresponding to the vertical vorticity extrema. This suggests that the flow is mainly horizontal and that the upwelling is negligible when compared to the motions associated with the primary dipole. Thus, the flow at the surface suggests that the dipolar vortex with Re=50 and $\delta=0.2$ remains Q2D during its lifetime.

Figure 4 shows the spanwise vorticity ω_y in the vertical symmetry plane of the dipolar vortex ($y=0$) at times $t=0.5$, 1, and 2 for the simulation with Re=50 and $\delta=0.2$ (δ^2 Re =2). From the contours of ω_y, it can be seen that the flow structure in the vertical symmetry plane barely changes in time. Only at early times ($t\approx0.5$), a small deviation from the initial shape is observed.

In Fig. 5, the 3D structure of half of the vortex dipole is illustrated by the $\lambda_2=0$ isosurface at time $t=1$ for two simulations: (a) one simulation with Re=50 and $\delta=0.2$ (δ^2 Re =2) and (b) one for Re=25 and $\delta=0.3$ (δ^2 Re=2.25). In this figure, it is clear that the vortex structure is 2D (independent of the vertical coordinate) even though the velocity field itself is 3D. All along its evolution, the dipolar vortex maintains this 2D structure. The described characteristics can also be observed for other small values of δ and similar values of δ^2 Re, as shown, for example, in Fig. 5 for the simulation with $\delta=0.3$ and δ^2 Re=2.25.

2. Transitional flow regime ($6\lesssim\delta^2$ Re$\lesssim$15)

Figure 6 shows the evolution of the dipolar vortex for a simulation with Re=200 and $\delta=0.2$ (δ^2 Re=8). Color/shade coding and black lines have the same meaning as in Fig. 3. As can be observed, the vorticity extrema no longer correspond with the primary vortex centroids. Instead, they are found at the front of the dipolar vortex and close to its symmetry axis. In the frontal region, the vertical vorticity extrema extend along the boundary of the dipolar vortex specially at late times (e.g., $t=1$ and $t=2$). However, the area bounded by the $\lambda_2=0$ isoline remains coherent.

In the lower row of Fig. 6, it can be seen that, as for the Q2D regime, there exist patches of positive divergence at the cores of the dipolar vortex. The presence of this horizontal divergence can be observed in the form of the flow lines spiraling out of the primary vortex centroids, suggesting the existence of a secondary flow that cannot be neglected. In addition, there exist two patches of converging flow (nega-

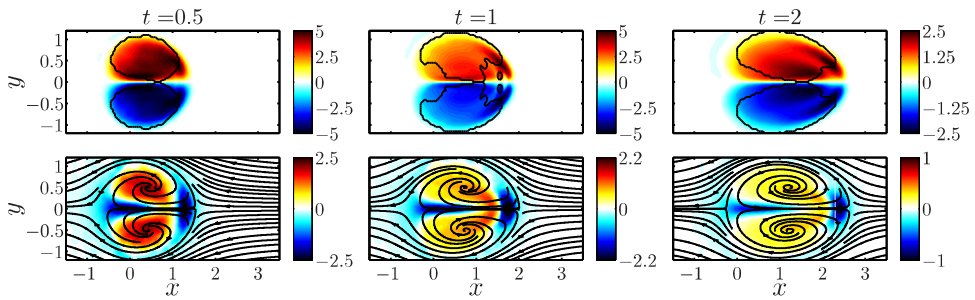

FIG. 6. (Color online) Same as in Fig. 3, except for a simulation with Re=200 and $\delta=0.2$ (δ^2 Re=8).

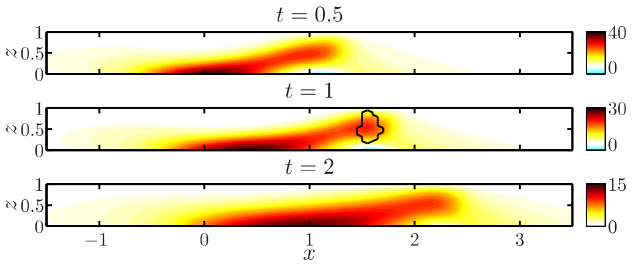

FIG. 7. (Color online) Same as in Fig. 4, except for the simulation with Re=200 and δ=0.2 (δ^2 Re=8). The black contour denotes the λ_2=0 isoline.

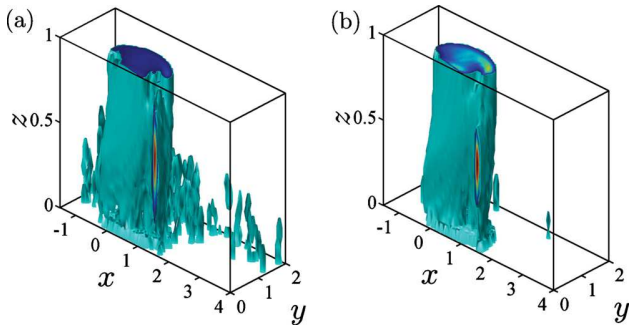

FIG. 8. (Color online) Same as in Fig. 5, except for the simulations with (a) Re=200 and δ=0.2 (δ^2 Re=8) and with (b) Re=89 and δ=0.3 (δ^2 Re=8).

tive horizontal divergence) corresponding to downwelling areas. These areas are found along the axis of the dipolar vortex as well as in front of the dipole. In the positive divergence areas, vertical vortex tubes just below the surface are compressed, while in the negative divergence areas, the vertical vortex tubes are stretched by the secondary motion. This stretching/compression mechanism is responsible for the local vorticity maxima in the negative divergence area.

Figure 7 shows the distribution of spanwise vorticity ω_y in the vertical symmetry plane of the vortex dipole (y=0) at times t=0.5, 1, and 2 for the simulation with Re=200 and δ=0.2 (δ^2 Re=8). In this flow regime, we observe a viscous boundary layer with high spanwise vorticity close to the bottom which is generated by the dipolar vortex propagating above the solid bottom. Then, fluid with high spanwise vorticity from the boundary layer is entrained toward the front of the dipole and forms a frontal circulation at mid-depth. In the current regime, this region of spanwise vorticity exists during most of the evolution, and at intermediate times ($t \approx 1$), a spanwise vortex is detected by the λ_2-criterion. The formation of the spanwise vortex can be partly attributed to vortex stretching in the spanwise direction, $\omega_y \partial v/\partial y$, which is of particular importance at the front of the dipole along its separatrix. Shortly after its appearance, the spanwise vortex vanishes as viscous effects start to dominate over vortex stretching due to decay of the dipolar vortex. At t=2, a patch of spanwise vorticity remains at the front of the dipole, but this vorticity patch is no longer a vortex.

Figure 8 shows the isosurface of the 3D λ_2-criterion for two simulations with δ^2 Re=8 and two different values of δ [(a) δ=0.2 and (b) δ=0.3] at time t=1. Here, the structure defined by the λ_2-criterion contains both the primary vortex and the spanwise vortex at the front of the dipole. In Fig. 8, the λ_2=0 isosurface is a coherent column as for the Q2D regime. However, the circular horizontal cross section is distorted due to the presence of the spanwise vortex and other 3D effects. In this figure, apparently, the flow structure is similar for different small values of δ and the same value of δ^2 Re.

3. 3D flow regime

Figure 9 shows the evolution of the dipolar vortex for the simulation with Re=500 and δ=0.2 (δ^2 Re=20). Color/shade coding and black lines have the same meaning as in Fig. 3. For this regime, as in the transitional one, the local vorticity extrema are found close to the symmetry axis of the dipolar vortex and at its front where they extend along its boundary. However, due to the stronger concentration of vorticity at the edges of the dipole, the λ_2=0 isoline at the surface loses its circular shape. In contrast, the boundary given by the λ_2-criterion becomes first an annulus and then an elongated structure which surrounds the centroids of the dipolar vortex. In this regime, the boundary of the vortices at the surface, given by the λ_2=0 isoline, indicates an important modification of the primary structure in comparison with the previous regimes.

In the lower row of Fig. 9, it can be seen that the horizontal divergence field is again composed of two patches of positive divergence in the cores of the dipolar vortex and two patches of converging flow: one along the axis of the dipolar vortex dipole and another at its front. As in the previous regime, the presence of this horizontal divergence can be observed in the form of the flow lines spiraling out of the primary vortex centroids, suggesting the existence of a secondary flow that cannot be neglected.

Figure 10 shows the distribution of spanwise vorticity ω_y in the vertical symmetry plane (y=0) of the vortex dipole at times t=0.5, 1, and 2 for the simulation with Re=500 and δ=0.2 (δ^2 Re=20). The magnitude of the spanwise vorticity in the vertical symmetry plane is much higher than the vertical vorticity of the primary vortex. As in the transitional regime, there is a viscous boundary layer close to the bottom below the primary vortex and a patch of spanwise vorticity ω_y at the front of the dipole at approximately mid-depth. The λ_2-criterion detects the presence of a spanwise vortex which develops after some time (see time t=1 and 2 in Fig. 10). In comparison to the transitional regime, the spanwise vortex is present for a longer time since viscous effects outside the boundary layer are negligible as compared with inertia forces for a longer time.

Figure 11 shows the λ_2=0 isosurface, outlining the boundary of the dipolar vortex for $y \geq 0$ at time t=1 for two simulations with δ^2 Re=20 and two different values of δ [(a) δ=0.2 and (b) δ=0.3]. For both simulations, the volume defined by the λ_2=0 isosurface contains again both the primary dipolar vortex and the spanwise vortex located at its front. It can be seen that in this regime, the 3D structure of the vortex depends strongly on the vertical direction: the shape is modified by the presence of the spanwise vortex at mid-depth, and at the top, the vortex core is hollow.

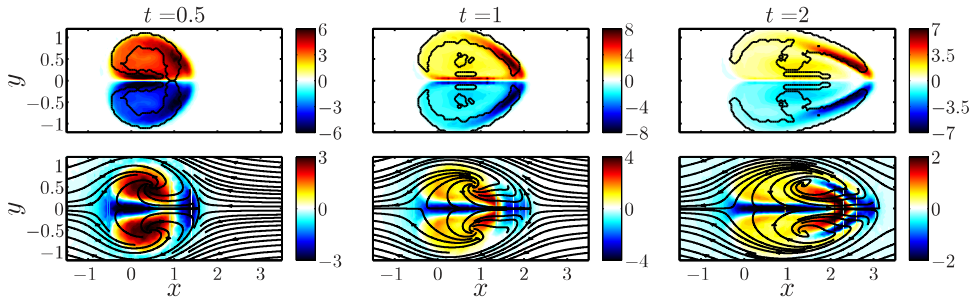

FIG. 9. (Color online) Same as in Fig. 3, except for a simulation with Re=500 and δ=0.2 (δ^2 Re=20).

IV. LABORATORY EXPERIMENTS

A. Experimental setup

The experimental setup, shown schematically in Fig. 12, consists of a water tank with a base of 50×50 cm^2. The tank is filled with a salt solution with a 178 g/l concentration up to a depth of 0.5 cm. To force the flow, two titanium electrodes are placed along two opposite sides of the tank, and one cylindrical magnet with a 2.5 cm diameter is placed underneath the tank bottom. An electric current is forced through the fluid using a power supply. Due to the interaction of this electric current and the magnetic field of the magnet, a Lorentz force is generated,

$$\boldsymbol{F}=\boldsymbol{J}\times\boldsymbol{B}, \tag{14}$$

with $\boldsymbol{J}$ the current density and $\boldsymbol{B}$ the magnetic field, by which the fluid is set in motion. In the current study, the fluid is forced for 1 s, and then it is left to evolve freely. The initial time t=0 is taken to be at the end of the forcing period. A similar forcing method has been previously used successfully to create dipolar vortices in a shallow fluid layer,[6,7] which have an initial radius similar to the diameter of the magnet: $R_0\approx2.5$ cm. In this way, the aspect ratio of the dipoles is $\delta\approx0.2$ for our experiments.

We consider the electric current to be homogeneous and running only in the y-direction, while the main component of the magnetic field above the center of the magnet is in the z-direction. Hence, the principal component of the Lorentz force is in the x-direction, thus forcing a dipolar vortex that propagates in this direction.

Particle image velocimetry (PIV) is used to measure the horizontal velocity field of the flow in a horizontal plane 3 mm above the bottom. The fluid is seeded with 106–150 μm polymethylmethacrylate particles which are illuminated with a double pulsed Nd:YAG laser sheet. Images of a 12×9 cm^2 area of the tank are taken using a Megaplus digital camera with a resolution of 1600×1200 pixels. Images at different time intervals are chosen, depending on the maximum velocity of the flow. These are then cross-correlated using PIV software from PIVTEC GmbH, Göttingen, Germany to calculate the horizontal velocity field.

In the current paper, results for three experiments are presented. These experiments were performed with three different magnitudes of the electric current, which resulted in three different values of the strength of the dipolar vortex. For the experiment with the lowest electric current, a picture was taken every 200 ms. Then, each picture was correlated with the following picture using the PIV software. For the experiments with moderate and strong forcing, a pair of images was taken every 1/15 s, with a time interval between each picture of 10 or 25 ms, depending on the magnitude of the electric current. Then each image pair was correlated. The three experiments presented in this paper correspond to Re$\approx$50, 160, 390 and they are representative of each of the three regimes described in the numerical study.

B. Experimental results

Figure 13 shows the vertical vorticity in the horizontal plane z=0.6 for three experiments at t=1. In this figure, the vortex dipole can be easily distinguished. However, the primary vortex dipole is surrounded by weak vorticity regions, which are typical of the forcing method employed and which are not found in the numerical simulations. Due also to the forcing method, the initial vertical profile of the horizontal velocity is not Poiseuille-like as in the simulations. Instead, the horizontal velocities are stronger close to the bottom than at the surface since the forcing is stronger closer to the magnet at the bottom.[6] In spite of these differences, the resulting evolution of the dipolar vortex in the laboratory experiments is in good agreement with the evolution of the dipolar vortex in the numerical simulations. This agreement indicates that the observed characteristics of the flow evolution do not depend critically on the precise form of the initial vertical profile. For example, it can be observed that the dipolar vortex remains coherent for small values of δ^2 Re (δ^2 Re$\approx$2.0), i.e., in the viscosity-dominated regime. For intermediate values of δ^2 Re (δ^2 Re$\approx$6.4), a slight elongation of the dipolar vor-

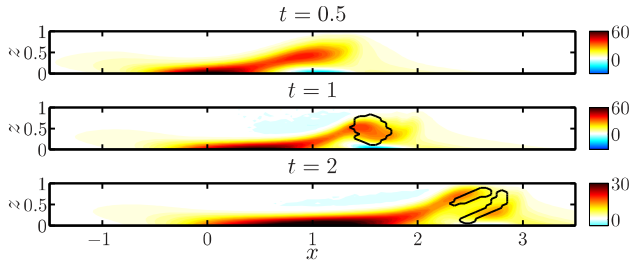

FIG. 10. (Color online) Same as in Fig. 4, except for a simulation with Re=500 and δ=0.2 (δ^2 Re=20). The black contour denotes the λ_2=0 isoline.

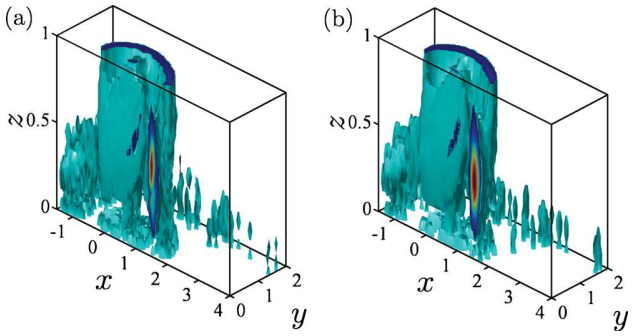

FIG. 11. (Color online) Same as in Fig. 5, except for the simulations with (a) Re=500 and δ=0.2 (δ^2 Re=20) and (b) Re=222 and δ=0.3 (δ^2 Re =20).

tex can be observed with bands of vertical vorticity maxima close to the symmetry axis of the dipole. Finally, for large values of δ^2 Re (δ^2 Re$\approx$15.6), the dipolar vortex is fully divided into a band of high vorticity at the front and patches of high vorticity close to the symmetry axis of the dipole.

Figure 14 shows the flow lines tangential to the horizontal velocity components in the reference frame comoving with the dipole and the horizontal divergence at t=1 for same three experiments as shown in Fig. 13. For δ^2 Re $\approx$2.0, the horizontal divergence is very small and beyond the accuracy of our measurements. Therefore, the horizontal divergence field is very noisy. On the other hand, for intermediate values of δ^2 Re (δ^2 Re$\approx$6.4), two patches of positive horizontal divergence in the primary vortex cores indicate an upwelling area as in the numerical simulations. Downwelling is clearly observed at the front and close to the symmetry axis of the dipolar vortex. For large values of δ^2 Re (δ^2 Re $\approx$15.6), the horizontal divergence distribution is the same as for intermediate values, except in the frontal region of the dipolar vortex. In this region, two narrow bands of horizontal divergence with opposite sign indicate the presence of a spanwise vortex. In addition, the flow lines clearly spiral out from the primary vortex centroids, indicating the presence of non-negligible secondary motions.

The generation mechanism used in the experiments does not seem to have a large effect on the overall characteristics of the flow evolution. For example, Lacaze *et al.*[8] performed one experiment where the dipole was generated using two closing flaps with δ=0.3 and δ^2 Re=20 (this is the same value of δ^2 Re used in the simulations presented for the 3D flow regime). In this experiment, the vorticity extrema were found in bands at the front of the dipole and close to its

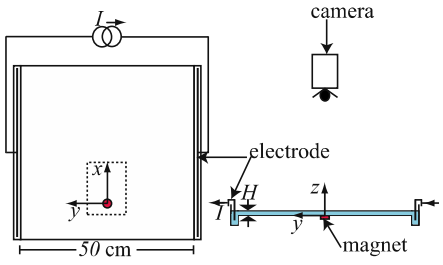

FIG. 12. (Color online) Schematic representation of the experimental setup.

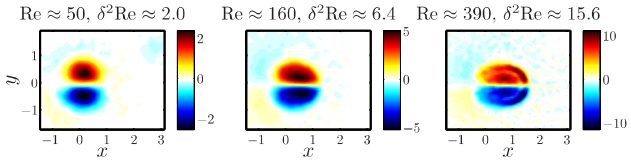

FIG. 13. (Color online) Vertical vorticity field in the horizontal plane z =0.6 (3 mm above the bottom) for three experiments at t=1. The color/shade denotes the vertical vorticity ω_z. The parameters for each experiment are shown above each panel.

symmetry axis, and a strong spanwise vortex developed like also observed in our experiments and numerical simulations.

We further characterize the flow by comparing the decay time τ_D of the vortex dipole with the Rayleigh decay time τ_R in the same way as it was done for the numerical simulations (see Fig. 15). The decay time for the Q2D flow (Re$\approx$50, δ^2 Re$\approx$2.0) is close to the Rayleigh decay time: $\tau_D \sim \tau_R/1.2$. However, as the Reynolds number increases and the flow becomes 3D, the decay time becomes much shorter: $\tau_D \sim \tau_R/1.6$ for Re$\approx$160 and $\tau_D \sim \tau_R/2.2$ for Re$\approx$390.

V. DISCUSSION AND CONCLUSIONS

In the last decade, several studies have shown different results about effect of shallowness on the two-dimensionalization of flows. A good example is found in the case of dipolar vortices.[3,4,6,7] On one side, shallowness seems to reduce vertical motions, but on the other side, complicated three-dimensional structures have been observed even for very shallow flows.

In the present work, we explain the apparently contradictory results from previous studies by performing a detailed exploration of the parameter space (Re, δ) both numerically and experimentally. It was found that the three-dimensionality of shallow dipolar vortices strongly depends on both the Reynolds number Re and the aspect ratio δ of the flow. However, for small values of δ (i.e., for shallow layers of fluid), the relative strength of the secondary motion only depends on the product δ^2 Re. This dependence on δ^2 Re and the existence of different flow regimes are in agreement with previous results for monopolar vortices.[10]

For shallow ($\delta \ll 1$) dipolar vortices, we observed three different regimes.

(1) *Q2D flow regime.* For low values of δ^2 Re (δ^2 Re$\lesssim$6), the flow is dominated by viscous effects and the secondary motions can be neglected. Note that, even if the

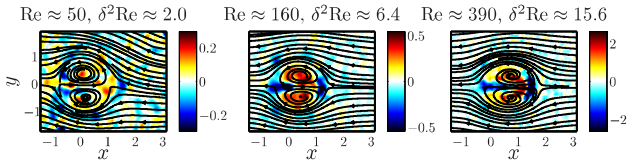

FIG. 14. (Color online) Horizontal divergence and flow lines tangential to the horizontal velocity components in the horizontal plane z=0.6 for three experiments at t=1. The color/shade denotes the horizontal divergence $\partial u/\partial x + \partial v/\partial y$. The parameters for each experiment are shown above each panel.

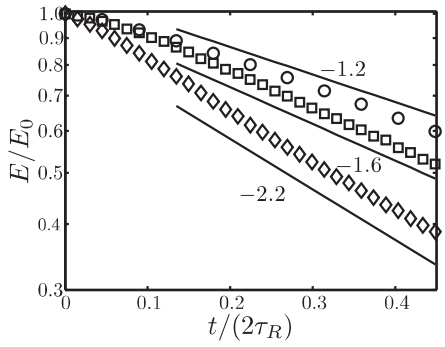

FIG. 15. Normalized kinetic energy in the horizontal plane z=0.6 as a function of time for the three experiments with $\delta \approx 0.2$, and Re≈50 (○), Re≈160 (□), and Re≈390 (◇). The solid lines are exponential fits.

velocity field is z-dependent, the three-dimensional structure of the dipolar vortex, given by the λ_2-criterion, is clearly 2D in this regime (see Fig. 5).

(2) *Transitional regime.* For intermediate values of δ^2 Re ($6 \lesssim \delta^2\,\mathrm{Re} \lesssim 15$), even if the vortex remains a coherent structure, secondary motions cannot be neglected since they modify the primary dipolar vortex. In addition, a spanwise vortex is observed at the front of the dipolar vortex. However, this spanwise vortex is not strong enough to endure the viscous effects for a long time.

(3) *3D regime.* For large values of δ^2 Re ($\delta^2\,\mathrm{Re} \gtrsim 15$), the distribution of the vertical vorticity component is intrinsically modified. The initial coherent horizontal distribution of vertical vorticity becomes "hollow," with the vorticity extrema close to the symmetry axis of the dipole and at its front. The overall structure of the dipole becomes three-dimensional due to strong secondary motions (both in the primary vortex cores and in the spanwise vortex located at the front of the dipole) which cannot be neglected.

The different initial conditions in both numerical and laboratory experiments result in small quantitative differences in the position of the transition regime in the parameter space. However, there is a strong qualitative similarity between experimentally and numerically obtained shallow ($\delta \ll 1$). This similarity suggests that the existence of the different regimes that depend only on the value of the parameter δ^2 Re is a robust property of shallow dipolar vortices, irrespective of the initial condition. A similar conclusion was reached for shallow monopolar vortices.[10] In this way, the three-dimensionalization of shallow flows depending on the parameter δ^2 Re seems to be valid for numerous kinds of shallow vortical flows.

ACKNOWLEDGMENTS

The authors are thankful to L. Lacaze for fruitful discussions, and they acknowledge support from O. Eiff and P. Brancher to carry out this research. M.D.M. also acknowledges financial support from CONACYT (Mexico) in the form of a graduate scholarship.

[1] G. H. Jirka, "Large scale flow structures and mixing processes in shallow flows," J. Hydraul. Res. **39**, 567 (2001).
[2] J. Pedlosky, *Geophysical Fluid Dynamics* (Springer-Verlag, New York, 1987).
[3] D. Sous, N. Bonneton, and J. Sommeria, "Turbulent vortex dipoles in a shallow water layer," Phys. Fluids **16**, 2886 (2004).
[4] D. Sous, N. Bonneton, and J. Sommeria, "Transition from deep to shallow water layer: formation of vortex dipoles," Eur. J. Mech. B/Fluids **24**, 19 (2005).
[5] J. C. Lin, M. Ozgoren, and D. Rockwell, "Space-time development of the onset of a shallow-water vortex," J. Fluid Mech. **485**, 33 (2003).
[6] R. A. D. Akkermans, L. P. J. Kamp, H. J. H. Clercx, and G. J. F. van Heijst, "Intrinsic three-dimensionality in electromagnetically driven shallow flows," Europhys. Lett. **83**, 24001 (2008).
[7] R. A. D. Akkermans, A. R. Cieslik, L. P. J. Kamp, R. R. Trieling, H. J. H. Clercx, and G. J. F. van Heijst, "The three-dimensional structure of an electromagnetically generated dipolar vortex in a shallow fluid layer," Phys. Fluids **20**, 116601 (2008).
[8] L. Lacaze, P. Brancher, O. Eiff, and L. Labat, "Experimental characterization of the 3D dynamics of a laminar shallow vortex dipole," Exp. Fluids **48**, 225 (2010).
[9] M. P. Satijn, A. W. Cense, R. Verzicco, H. J. H. Clercx, and G. J. F. van Heijst, "Three-dimensional structure and decay properties of vortices in shallow fluid layers," Phys. Fluids **13**, 1932 (2001).
[10] M. Duran-Matute, L. P. J. Kamp, R. R. Trieling, and G. J. F. van Heijst, "Scaling of decaying shallow axisymmetric swirl flows," J. Fluid Mech. **648**, 471 (2010).
[11] J. Jeong and F. Hussain, "On the identification of a vortex," J. Fluid Mech. **285**, 69 (1995).
[12] J. Z. Wu, H. Y. Ma, and M. D. Zhou, *Vorticity and Vortex Dynamics* (Springer, Heidelberg, 2006).
[13] H. Lamb, *Hydrodynamics* (Cambridge University Press, Cambridge, 1932).
[14] COMSOL 3.5 User's Guide, COMSOL AB, Tegnérgatan 23, SE-111 40 Stockholm, Sweden, available as of May 2008 at http:www.comsol.com.
[15] V. V. Meleshko and G. J. F. van Heijst, "On Chaplygin's investigations of two-dimensional vortex structures in an inviscid fluid," J. Fluid Mech. **272**, 157 (1994).
[16] J. B. Flòr and G. J. F. van Heijst, "An experimental study of dipolar vortex structures in a stratified fluid," J. Fluid Mech. **279**, 101 (1994).
[17] P. Billant and J. M. Chomaz, "Experimental evidence for a new instability of a vertical columnar vortex pair in a strongly stratified fluid," J. Fluid Mech. **418**, 167 (2000).
[18] D. Sipp, L. Jacquin, and C. Cossu, "Self-adaptation and viscous selection in concentrated two-dimensional vortex dipoes," Phys. Fluids **12**, 245 (2000).
[19] J. Paret, D. Marteau, O. Paireau, and P. Tabeling, "Are flows electromagnetically forced in thin stratified layer two-dimensional?," Phys. Fluids **9**, 3102 (1997).
[20] U. T. Bödewadt, "Die Drehströmung über festem Grunde," Z. Angew. Math. Mech. **20**, 241 (1940).